The Kinetics and Mechanism of the Pyrite-to-Pyrrhotite Transformation

J.M. LAMBERT, JR., G. SIMKOVICH, and P.L. WALKER, JR.

The kinetics of the transformation of pyrite to pyrrhotite have been investigated. The study was performed using thermogravimetric analysis over the temperature range of 620 to 973 K in atmospheres of H_2, He, Ar, and *in vacuo* over a wide range of pressures: 0.20 Pa to 4.24 MPa. Based on the kinetic results, a mechanistic picture of the various steps exerting control over the transformation is proposed. The thermal decomposition proceeds *via* a two-step, consecutive process. The rate-controlling step is the desorption of sulfur vapor from the surface. The presence of H_2 introduces different rate-controlling steps into the sequence, providing the H_2 exists at a pressure sufficiently high to suppress the rate of thermal decomposition. Rates at which the H_2 reduction occurs with pyrite samples from different sources depends upon the samples' impurity level and the extent to which various crystallographic faces are exposed.

I. INTRODUCTION

THE thermal decomposition of pyrite (FeS_2) has been investigated by many researchers. The apparent activation energy for the decomposition has been reported in the range of 120 to 275 kJ/mol.[1–3] The rate-determining step has been attributed by previous researchers to the dissociation of an S_2^* anion,[1] the coordinated lattice destruction,[1] the movement of the pyrite/pyrrhotite interface,[2] and gaseous diffusion.[3]

The kinetics of the reduction of pyrite in H_2 has also been investigated by many researchers.[1,4–10] They have reported apparent activation energies for the reduction between 70 and 200 kJ/mol. Most authors have reported that in the presence of H_2, FeS_2 is converted to FeS with the production of H_2S. Few authors have attempted to include the fact that FeS_2 is not converted directly to FeS and have neglected to account for the intermediate pyrrhotites which form during the reduction. One author[9] has proposed the following mechanism:

$$2FeS_2 + H_2 \longrightarrow Fe_2S_3 + H_2S \quad [1]$$

$$Fe_2S_3 + H_2 \longleftrightarrow 2FeS + H_2S \quad [2]$$

The formation of Fe_2S_3 is unlikely based on present knowledge of the thermodynamics stability of iron sulfides.[11–14]

Another, somewhat more plausible, mechanism has been suggested by Niwa *et al.*:[10]

$$FeS_2 + H_2 \longrightarrow FeS + H_2S \quad [3]$$

$$FeS + xS \text{ (in } FeS_2) \longrightarrow FeS_{1+x} \quad [4]$$

$$FeS_{1+x} + xH_2 \longrightarrow FeS + xH_2S \quad [5]$$

These authors defined FeS_{1+x} to be $FeS_{1.15}$ based on their experimental observation that this was the only pyrrhotite which appeared. They further concluded that the second reaction was rapid compared to the other two, since no FeS appeared when FeS_2 was present. An apparent activation energy of 120 kJ/mol was reported.

Other authors,[7,9] who also reported the apparent activation energy for the reduction to be 100 kJ/mol, concluded that the rate was controlled by the diffusion of sulfur in the pyrite lattice and by the availability of H_2 to remove sulfur from the pyrite surface. They proposed the following two-step mechanism:

$$FeS_2 \longrightarrow FeS + S \quad [6]$$

$$S + H_2 \longrightarrow H_2S \quad [7]$$

It is the purpose of this investigation to determine the rate and mechanism by which pyrite is reduced to pyrrhotite both thermally and in H_2, and to attempt to elucidate the cause of the widely varying activation energies reported in the literature for this transformation.

II. THEORETICAL CONSIDERATIONS

Prior to beginning the experimental work, the thermodynamic region of stability was examined to establish the limits within which the kinetics were to be investigated. According to accepted phase equilibria of iron-sulfides,[11] pyrite (FeS_2) decomposes to pyrrhotite (FeS_x, $1.00 < x < 1.23$) in the temperature range of 523 to 1016 K. As can be seen in Figure 1, the composition of the pyrrhotite in equilibrium with pyrite is dependent upon the temperature.

Employing the thermodynamic data of Toulmin and Barton[12] and the description of the pyrite/pyrrhotite solvus according to Scott and Barnes,[13] the composition of pyrrhotite in equilibrium with pyrite can be obtained as a function of temperature. This relationship can be seen in Figure 2. The nearly linear region extending up to approximately 820 K can be expressed by the following equation:

$$x \text{ in } FeS_x = 1.45 \times 10^{-4} (T) + 1.0354 \quad [8]$$

where T is the temperature in kelvin. An equation describing the entire range is given by the following polynomial:

J.M. LAMBERT, Jr., Engineer, is with the Parr Instrument Company, Moline, IL 61265. G. SIMKOVICH and P.L. WALKER, Jr., Professors Emeriti, are with the Department of Materials Science and Engineering, The Pennsylvania State University, University Park, PA 16802.

Manuscript submitted February 10, 1997.

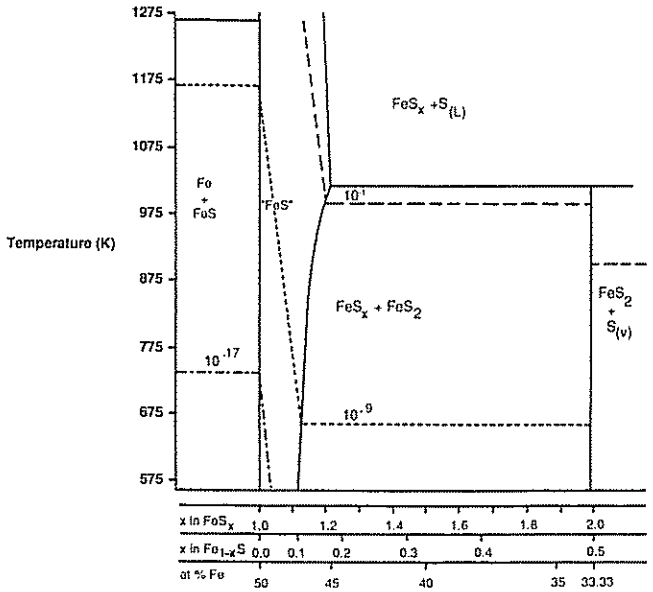

Fig. 1—High-temperature Fe-S phase diagram with isobars of equilibrium sulfur pressure (MPa).

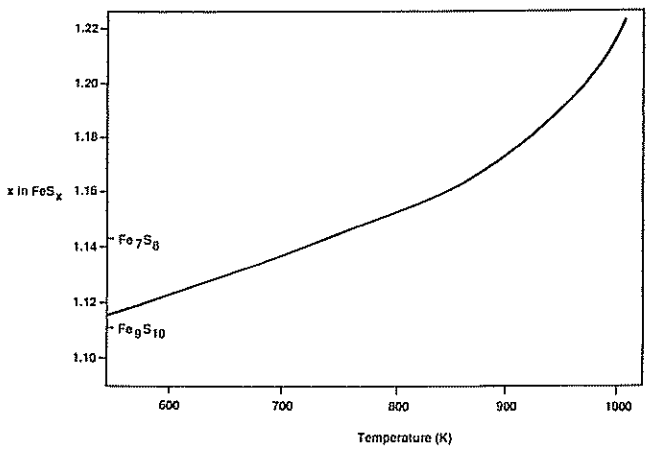

Fig. 2—Composition of pyrrhotite in equilibrium with pyrite as a function of temperature.

$$X \text{ in } FeS_x = 4.3739 \times 10^{-12} (T)^4 - 1.2034 \times 10^{-8} (T)^3 + 1.2365 \times 10^{-5} (T)^2 - 5.4779 \times 10^{-3} (T) + 1.9900 \quad [9]$$

where, again, T is temperature in kelvin.

These empirical equations describe the composition of the pyrrhotite into which pyrite will first decompose. The pyrrhotite can be reduced further toward troilite (stoichiometric FeS) and, eventually, iron. The compound whose composition lies between troilite and the pyrrhotite in equilibrium with pyrite is a solid solution of sulfur in troilite. Any pyrrhotite stoichiometry within this range will form a stable compound, provided an appropriate sulfur fugacity exists in equilibrium with it.[12,14]

III. EXPERIMENTAL

Pyrite from Sonora, Mexico was obtained from Ward's Natural Science Establishment (Rochester, NY). The pyrite

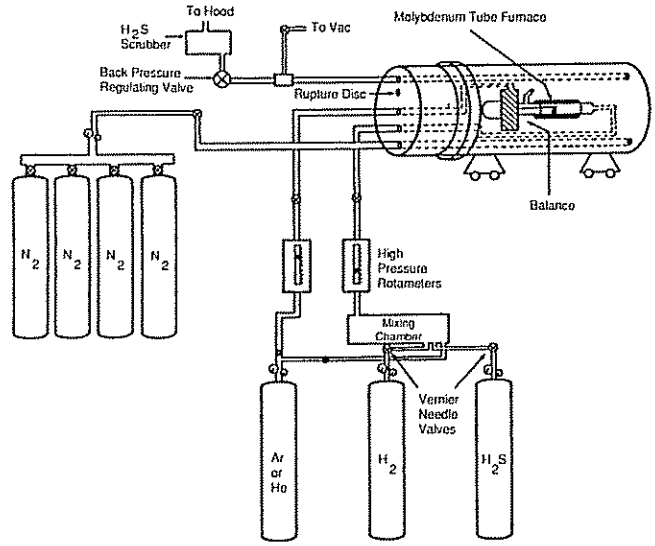

Fig. 3—Experimental thermogravimetric system.

was ground to a 210 × 250-μm particle size in a ceramic ball mill. The ground pyrite was washed in 2N HCl to remove surface oxides and ball mill tailings. After a thorough rinsing with distilled water, the samples were stored under vacuum until use.

Characterization of the pyrite by X-ray powder diffraction revealed no impurities, and the very narrow peak widths observed indicated a crystallite size greater than 100 nm. Spectroscopic analysis showed no minor impurities and only a trace (<100 ppm) of Co and Cu. None of the following elements were detected: Ag, Al, B, Be, Bi, Ca, Cd, Cr, Ge, In, La, Mg, Mn, Ni, Pb, Sc, Sn, Ti, V, Y, or Zr. A density of 5.01 g/cc was determined by a helium displacement technique.

The extent of decomposition was measured on a thermogravimetric balance (Du Pont 951) mounted inside an Autoclave Engineers' (Erie, PA) pressure containment vessel, as shown in Figure 3. The system was operated by first evacuating the contents of the vessel with a mechanical roughing pump and then pressurizing the system to the desired level with N_2. A constant purge rate was established with the aid of the backpressure regulation valve (Tescom, Elk River, MN). The N_2 within the reaction tube was displaced by flowing the desired reaction atmosphere into the tube at a pressure slightly positive to the vessel pressure. The reaction products exit the reaction tube and enter the N_2-filled area surrounding the balance. From here they are purged along with the N_2. The reaction temperature is maintained to within 5 K by a programmable temperature controller (West, Minneapolis, MN) and a hand-wound molybdenum furnace operated at 220 V.

A typical experiment employed a sample size of 4 mg pyrite. The system was purged with N_2, evacuated to 0.2 Pa, and then pressurized to the desired experimental operating level. The reaction atmospheres were introduced at a constant flow rate of 300 cc/min (NTP). This rate was chosen to minimize both the stagnant boundary layer thickness, thereby maximizing the removal of reaction products, and any possible buoyancy effects within the reactor tube. The temperature was increased at a rate of 15 K/min and then held isothermally at the desired temperature. The sample

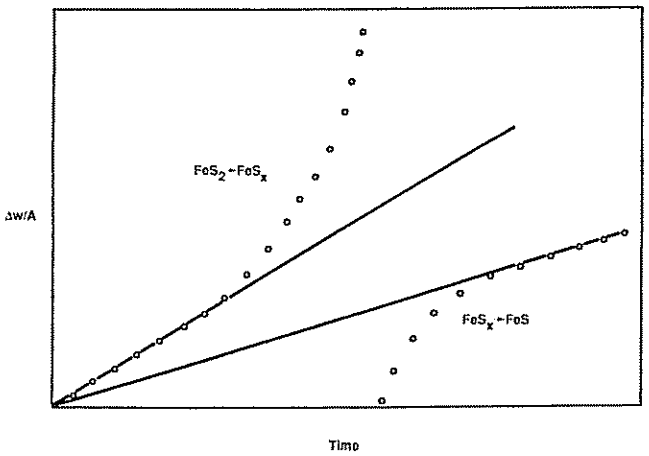

Fig. 4—Typical analysis of consecutive two-step reactions by shrinking-core model.

weight and temperature, as measured by a type-K thermocouple placed in close proximity to the sample, were recorded on a dual-pen recorder (Du Pont 990).

IV. RESULTS AND DISCUSSION

A. *Kinetic Analyses*

1. *Thermal reduction*

A first series of experiments was conducted *in vacuo*, without a flowing gas atmosphere. The system was purged with N_2 and evacuated, as described previously, but pressurization was not begun. The system was allowed to remain under evacuation at a pressure of approximately 0.2 Pa. Under these conditions, the sulfur pressure cannot be reduced to the extent required to allow the formation of iron. Thus, pyrite will undergo two sequential reactions, each liberating sulfur vapor: $FeS_2 \rightarrow FeS_x$ and $FeS_x \rightarrow FeS$. The composition of the intermediate pyrrhotite can be obtained from Eq. [8] or [9] as a function of temperature. The data from ten experiments were analyzed in the manner described subsequently.

Since heterogeneous, gas/solid reactions take place at the surface of the solid, the weight loss per unit time is proportional to the surface area present at time t. This can be expressed as

$$\Delta w / \Delta t = \delta A \qquad [10]$$

Rearrangement of this expression shows that a plot of $\Delta w/A$ *vs* time will give a straight line whose slope is the constant of proportionality (δ). Assuming the reaction to be first order, the constant of proportionality (δ) is equivalent to the specific reaction rate (R_s).

Pyrite decomposition appeared to commence on the exterior surface and progress inwardly. It was therefore assumed that the reaction $FeS_2 \rightarrow FeS_x$ could best be described by a shrinking-core model.[15] Application of Eq. [10] to a shrinking-core model dictates that an expression be found to describe the change in area (A) as a function of time or extent of reaction.

By assuming spherical geometry, the surface area present at time t can be expressed as

$$A = 4\pi [r (1 - f)]^2 \qquad [11]$$

where r is the initial particle radius and f is the fraction of this radius which has reacted at time t. From geometrical considerations, it can be shown that

$$(1 - f) = (1 - X)^{1/3} \qquad [12]$$

where X is the fractional conversion of reactant into product. Combining Eqs. [11] and [12], the surface area is

$$A = 4\pi [r (1 - X)^{1/3}]^2 \qquad [13]$$

$$\text{or } A = 4\pi r^2 (1 - X)^{2/3} \qquad [14]$$

$$\text{or } A = A_0 (1 - X)^{2/3} \qquad [15]$$

where A_0 is the original surface area at time $t = 0$. The fractional conversion X is defined as

$$X = \Delta w / \alpha w_0 \qquad [16]$$

where Δw is the weight loss at time t, w_0 is the original sample weight, and α is the fraction of w_0 lost when $X = 1.0$. The value of α can be obtained from the composition of the pyrrhotite into which the pyrite first decomposes:

$$\alpha = (2 - x) \left[\frac{\text{atomic weight of S}}{\text{molecular weight of } FeS_2} \right] \qquad [17]$$

$$\text{or } \alpha = (2 - x)\ (0.267) \qquad [18]$$

where x is the x in FeS_x, as calculated from Eq. [8] or [9].

By combining Eqs. [15] and [16], the weight loss per unit area is found to be

$$\frac{\Delta w}{A} = \frac{\Delta w}{A_0 (1 - X)^{2/3}} = \frac{\Delta w}{A_0} \left[1 - \frac{\Delta w}{\alpha w_0} \right]^{-2/3} \qquad [19]$$

The value of A_0 can be obtained from the product of w_0 and the specific surface area as calculated from the BET equation, using Kr adsorption data obtained at 77 K. The specific surface area of 210 × 250-μm pyrite was 0.17 cm^2/mg.[16] The kinetics of the reaction $FeS_2 \rightarrow FeS_x$ can be described by plotting $\Delta w/A$ from Eq. [19] *vs* time. The slope of such a plot is the specific reaction rate (R_s).

The second reaction, $FeS_x \rightarrow FeS$, was not assumed to follow a shrinking-core model, since no evidence was available to justify its use. The data were analyzed on a simple weight loss per unit area basis, in accordance with Eq. [10]. A constant specific surface area was assumed. The specific surface areas of the pyrrhotites were measured by Kr adsorption at 77 K and were found to be dependent upon the reaction temperature.[16] The area of pyrrhotite present at time t, to be used in the kinetic analyses, was calculated by multiplying the weight of pyrrhotite present by the specific surface area found for that pyrrhotite at the particular temperature of reaction. A plot of $\Delta w/A$ *vs* t was then constructed with the specific reaction rate (R_s) equal to the slope of the plot.

A typical example of the $\Delta w/A$ *vs* t plots for both reactions is shown in Figure 4. Because the weight loss data from the thermogravimetric analysis (TGA) include both reactions, the straight line expected from analysis of the first reaction deviated upward as the conversion approached unity. Similarly, the analysis of the second reaction showed downward deviation as zero conversion is approached. It was therefore assumed that in the early stages, the observed weight loss was due primarily to the $FeS_2 \rightarrow FeS_x$ reaction;

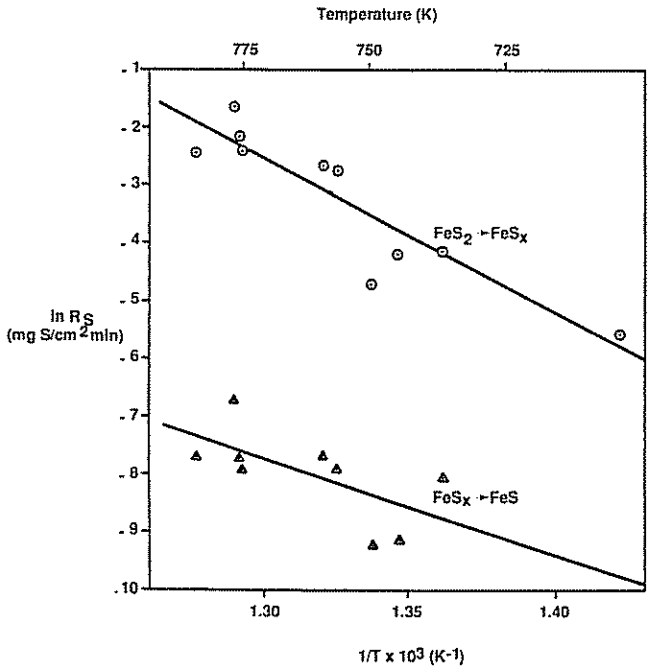

Fig. 5—Arrhenius plot of vacuum decomposition of 210 × 250-μm Sonora pyrite particles.

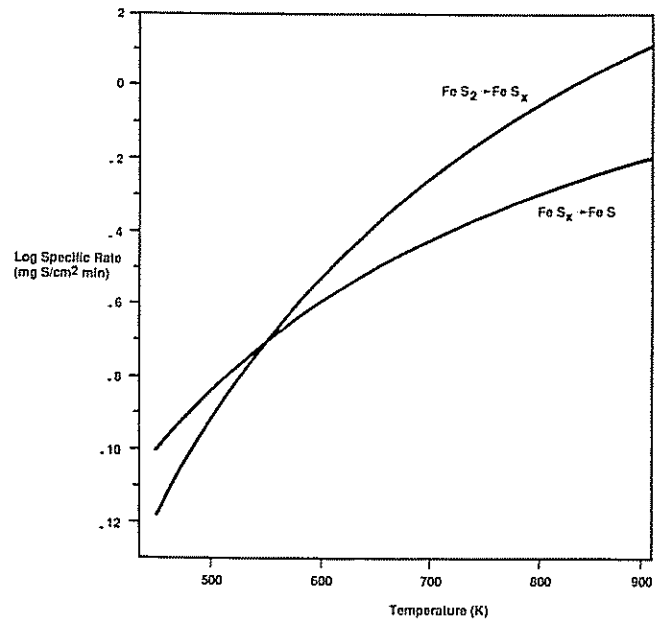

Fig. 6—Variation in rates of first and second reaction steps as a function of temperature.

and during the latter stages of data collection, the observed weight loss was due to the $FeS_x \rightarrow FeS$ reaction. Slopes of the straight lines shown in Figure 4 were taken as the specific reaction rates for the two sequential reactions.

The natural logarithms of the specific reaction rates were plotted *vs* the reciprocals of the absolute reaction temperatures, as shown in Figure 5. From this figure, Arrhenius parameters can be obtained which describe the specific rate given by the expression $R_s = R_{s,0} \exp(-E_{act}/RT)$. The pre-exponential term ($R_{s,0}$) for the first reaction was found to be 8.9×10^{13} mg/cm min, and the apparent activation energy (E_{act}) was found to be 222 kJ/mol. The standard deviation in this activation energy was 38 kJ/mol. For the second reaction, $FeS_x \rightarrow FeS$, the parameters were found to be $R_{s,0} = 1.1 \times 10^6$ mg/cm^2 min and $E_{act} = 139$ kJ/mol with a standard deviation of 63 kJ/mol.

The scatter in the data is believed to be due primarily to experimental design. The TGA system used in these experiments was designed to be operated at elevated pressures, not under vacuum conditions. It is doubtful that the pressure of 0.2 Pa was maintained exactly throughout the duration of all experiments.

It is informative, however, to plot these calculated rates as a function of temperature, as shown in Figure 6. It can be seen that at the higher temperatures, the rate of the $FeS_2 \rightarrow FeS_x$ reaction is much faster than the $FeS_x \rightarrow FeS$ reaction. At the lower temperatures, the two rates become more identical. Based on this analysis and knowledge of the thermodynamic limitations, it is predicted that if two samples of pyrite were to undergo identical extents of weight loss at two different temperatures, the resultant pyrrhotites would differ in two ways: composition and amount.

According to Figure 1, the composition of pyrrhotite in equilibrium with pyrite varies with temperature. The value of x in FeS_x increases with increasing temperature. Thus, compared to a pyrrhotite formed at a lower temperature, the FeS_x formed at the higher temperature will be richer in sulfur. As this pyrrhotite undergoes subsequent reduction through the solid-solution region toward troilite, it loses sulfur, forming a second pyrrhotite phase which is referred to here as "FeS." Figure 6 shows that at very high temperatures, the $FeS_2 \rightarrow FeS_x$ reaction is much faster than the $FeS_x \rightarrow FeS$ reaction. Thus, for a given extent of weight loss at very high temperatures, only a small amount of the FeS phase would be expected to form. Most of the weight loss will be due to the more rapid $FeS_2 \rightarrow FeS_x$ reaction. This is shown schematically in Figure 7. At lower temperatures, a longer period of time will be required to achieve the same given extent of weight loss. Under these conditions, Figure 6 shows that the two reaction rates are more identical. Thus, at lower temperatures, more of the FeS phase will have had time to form. The ratio of the amount of FeS to the amount of FeS_x formed will be greater at lower temperatures than at higher temperatures. This is also shown schematically in Figure 7.

To confirm this interpretation and to lend credence to the proposed kinetic analysis, an experiment was performed by reducing two samples of pyrite under the previously described vacuum conditions at 698 and 808 K. The composition and amounts of the resultant pyrrhotites were determined by an X-ray diffraction technique.[14]

The results of this analysis are shown in Table I, where the compositions are given as x in FeS_x and the amounts are reported as the X-ray diffractogram peak areas. It can be seen, first, that two distinct pyrrhotites were observed at each temperature. The composition of the higher sulfur pyrrhotite formed in each case agrees well with the composition predicted by Eq. [8] or [9] for a pyrrhotite in equilibrium with pyrite. The other pyrrhotite phase produced at each temperature was found to be of a lower sulfur content. This agrees with the proposed two-step, consecutive reaction scheme.

Comparing the composition of the two FeS phases, it is seen that less sulfur appears in the pyrrhotite produced at

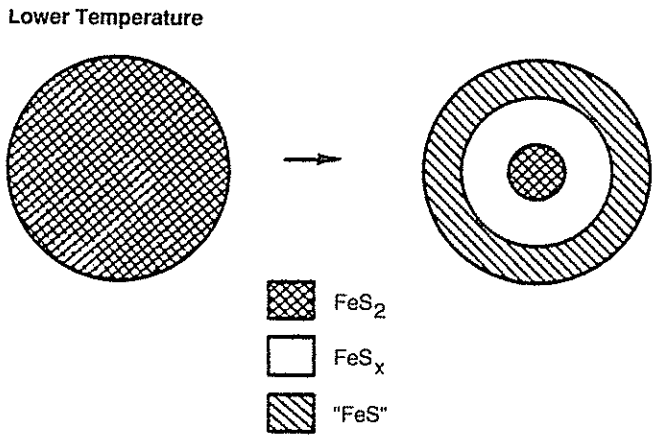

Fig. 7—Schematic illustration of pyrite decomposition at different temperatures.

Table I. X-Ray Analysis of Vacuum-Reduced 210 × 250-μm Sonora Pyrite

Temperature (K)	Weight Loss (Pct)	Calculated x in FeS_x	Experimental x in FeS_x	Peak Area	x in FeS_x*	Peak Area*
698	11	1.137	1.140	2.3	1.090	10.8
808	18	1.153	1.152	7.5	1.105	7.9

*This pyrrhotite is referred to as "FeS" in the text and in Figs. 1 and 7.

a lower temperature. This is predicted, since the FeS_x phase formed at the lower temperature would have had a longer time to undergo subsequent reduction before the given extent of weight loss was achieved.

Along with greater reduction to a pyrrhotite of a lower sulfur content, it was predicted that the ratio of the amount of FeS formed to the amount of FeS_x formed would be greater at the lower temperature. Comparison of the peak areas in Table I shows that such was the case. At 808 K, nearly equal amounts of FeS and FeS_x were found. At the lower temperature, 698 K, the ratio of amounts formed was 4.7, also in agreement with the proposed scheme.

Although the data shown in Figure 5 exhibit a fair amount of scatter, the preceding experiment does lend credence to the proposed kinetic scheme: pyrite first decomposes to a pyrrhotite whose composition can be calculated from thermodynamic data. This pyrrhotite is subsequently reduced further through the region of solid solution to eventually form troilite. It therefore appears reasonable to assume that a significant sulfur fugacity exists in the interior of the particle. If such a fugacity did not exist, only one

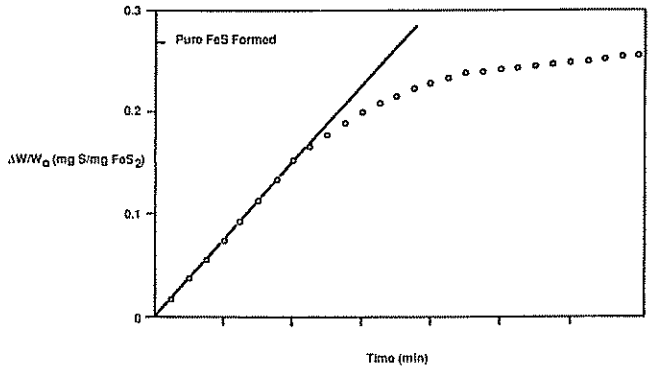

Fig. 8—Typical analysis of pyrite decomposition by initial slope method.

pyrrhotite would have been observed in the X-ray diffraction analyses.

An alternative method of obtaining the kinetic results is to simply plot the fractional weight loss (observed weight loss divided by the original weight) *vs* time. The initial slopes of these plots are then divided by the surface areas of the starting pyrite to obtain the specific reaction rate. This "initial slope" method of calculating R_S precludes analysis of the second reaction, $FeS_x \rightarrow FeS$. However, since it is the first reaction, $FeS_2 \rightarrow FeS_x$, which is of primary concern in this investigation, this method was chosen for all subsequent analyses of pyrite decomposition. A graphic example of this method is shown in Figure 8.

Results of the *in vacuo* experiments described previously, now analyzed by the initial slope method, are plotted in Arrhenius fashion in Figure 9. From this figure, the kinetic parameters were found to be $R_{s,0} = 1.3 \times 10^{12}$ mg/cm² min and $E_{act} = 198$ kJ/mol with a standard deviation of 31 kJ/mol. This agrees, within experimental error, with the value obtained by the previous method of analysis shown in Figure 5 ($E_{act} = 222$ kJ/mol, ±38 kJ/mol).

The thermal decomposition of Sonora pyrite was also investigated in inert gaseous atmospheres. Twelve experiments using particles of 210 × 250 μm in size were performed in He at ambient pressure (0.1 MPa). Analysis by the initial slope method gave the Arrhenius plot shown in Figure 10. From this figure, a pre-exponential factor of 2.2×10^{12} mg/cm² min and an apparent activation energy of 217 kJ/mol (standard deviation = 13 kJ/mol) were obtained.

Four experiments were also performed using Sonora pyrite particles of 210 × 250 μm in size in 0.1 MPa of Ar. The initial slope analysis gave the Arrhenius plot shown in Figure 11. From this plot, it was found that $R_{s,0} = 7.3 \times 10^{10}$ mg/cm² min and $E_{act} = 192$ kJ/mol (standard deviation = 23 kJ/mol).

It can be noted that the apparent activation energies for pyrite decomposition under all three conditions, *in vacuo* and at ambient pressures of He and Ar, were found to be identical (within experimental limits). This may be interpreted to imply that the rate-determining step in all cases was the same. Since the rate of thermal decomposition was reduced with increasing pressure, the rate-determining step is thought to be the surface reaction of sulfur atoms combining to form an adsorbed S_2 molecule, or the subsequent desorption of this S_2 molecule. Since the measured rates were found to be different in He than in Ar, the desorption

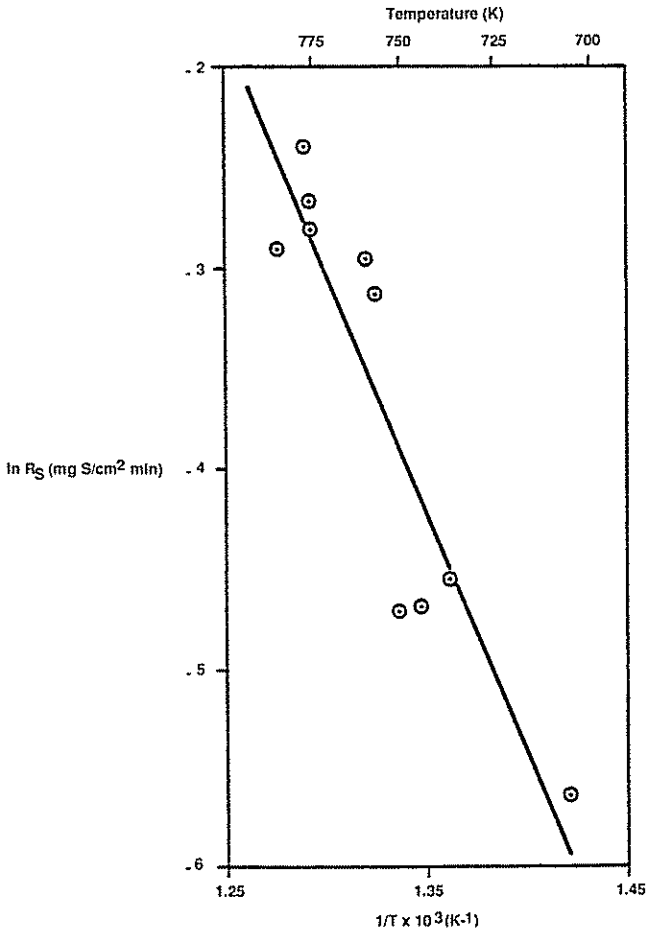

Fig. 9—Arrhenius plot of vacuum decomposition of 210 × 250-μm Sonora pyrite analyzed by the initial slope method.

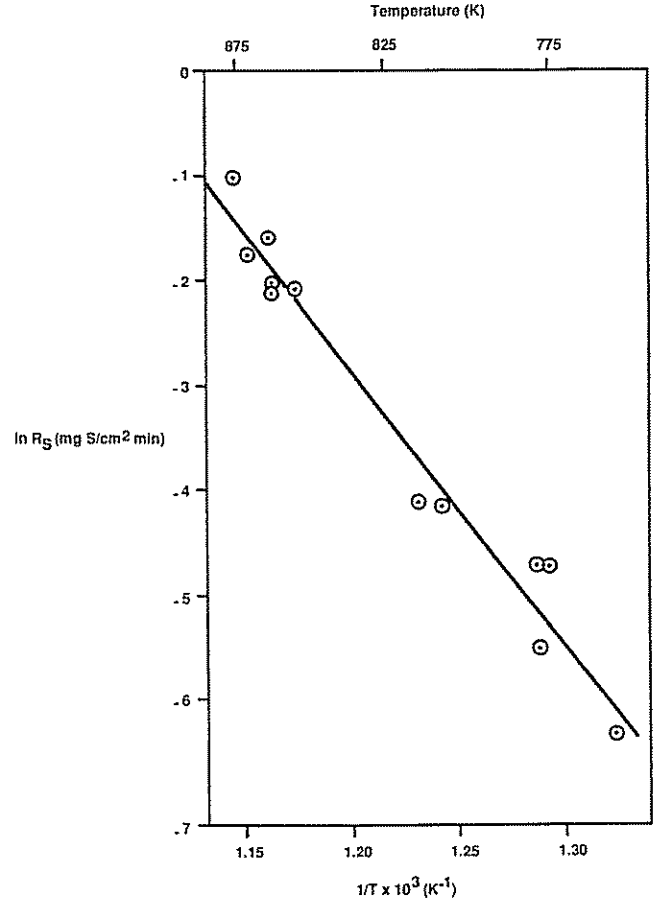

Fig. 10—Arrhenius plot of 210 × 250-μm Sonora pyrite decomposition in He at 0.1 MPa (1 atm).

of S_2 is the more likely choice for the rate-determining step. The atmosphere in the stagnant boundary layer next to the particle surface will have a higher S_2 concentration when transport away from the particle is restricted. This will result in a higher recondensation rate, thus leading to a decrease in the net rate of pyrite reduction observed with the TGA technique.

The extent to which transport across the boundary layer is restricted is dependent upon the ratio D/d, where D is the diffusion coefficient of sulfur vapor (S_2) through the gas present and d is the boundary layer thickness.[17] Values of D, calculated by the method of Satterfield and Sherwood,[18] and d, calculated by the method of Turkdogan *et al.*,[19] yield values of $(D/d)_{Ar}/(D/d)_{He}$ greater than 1 over the temperature range studied and at 0.1 MPa Ar and He pressure. Thus, more rapid weight loss in Ar than in He is expected, consistent with the experimental results.

Increasing the pressure of He and Ar, while maintaining the flow rate constant at 300 cc/min (NPT), will obviously reduce the net rate of sulfur evaporation from the surface. Figure 12 presents results for the reduction of 210 × 250 μm particles of Sonora pyrite in the presence of 0.8 MPa of He and Ar. The rate of pyrite decomposition was greatly reduced from that found at ambient pressure. Kinetic parameters obtained from Figure 12 are summarized in Table II. Note that the apparent activation energy associated with the specific reaction rate is higher when operating at elevated pressures.

2. *Hydrogen Reduction*

Data from 17 experiments performed with Sonora pyrite in 0.1 MPa flowing H_2 are shown in Figure 13. The Arrhenius plot can be divided into three distinct regions. The kinetic parameters for these three regions are listed in Table III.

As is discussed in more detail elsewhere,[20] an Arrhenius plot showing distinct breaks in slope, with the slope decreasing with increasing temperature, is consistent with pathways comprised of reactions occurring in series; whereas, a plot with distinct breaks in slope, with the slope increasing with increasing reaction temperature, is consistent with parallel reaction pathways. From the high-temperature region of Figure 13, an apparent activation energy of 195 kJ/mol was calculated. This corresponds well with the activation energy found for the thermal decomposition of pyrite. It is concluded that at high temperatures, the rate at which sulfur is leaving the particle precludes the inward diffusion of H_2, and the measured reaction rate is dominated, not by hydrogen reduction, but by the parallel pathway of thermal decomposition.

Additional evidence supporting this view was obtained during another flowing H_2 experiment, while attempting to achieve an isothermal reaction temperature of 973 K. The excessive weight loss experienced before reaching the de-

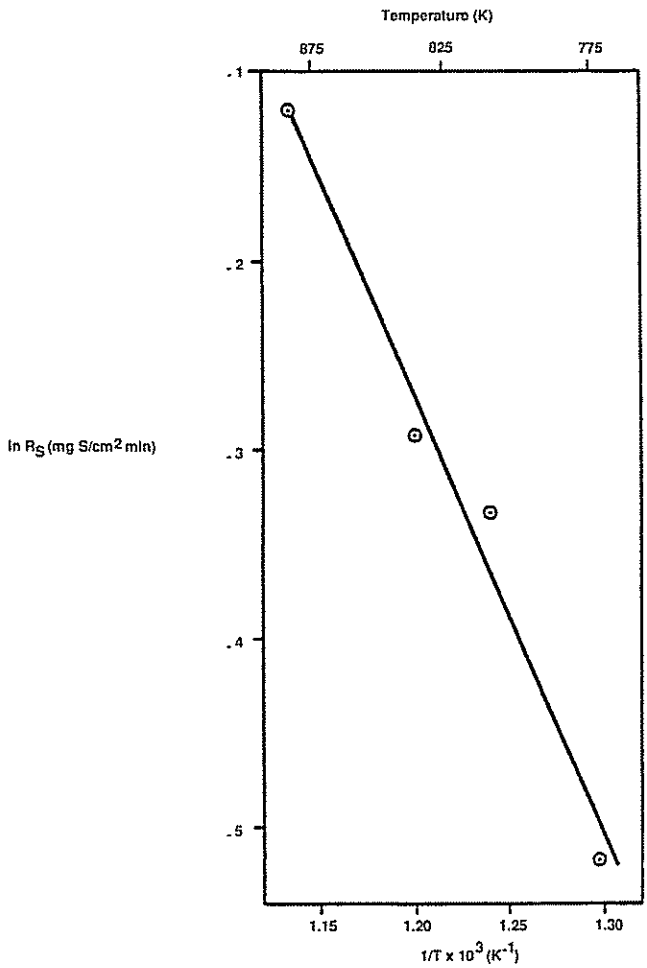

Fig. 11—Arrhenius plot of 210 × 250-μm Sonora pyrite decomposition in Ar at 0.1 MPa (1 atm).

Table II. Kinetic Parameters for the Decomposition of 210 × 250-μm Sonora Pyrite at 0.8 MPa of Helium and Argon

Atm	$R_{x,0}$ (mg/cm^2 min)	E_{act} (kJ/mol)	Standard Deviation (kJ/mol)
He	7.1×10^{16}	294	14
Ar	8.7×10^{15}	275	13

sired temperature forbid accurate kinetic analysis, but it was noticed that a yellow solid was deposited on the cold region of the reactor exit tube. Analysis by X-ray diffraction confirmed that the deposit was sulfur. Since higher temperatures would shift the $H_2 + S \rightarrow H_2S$ reaction equilibrium in favor of H_2S and not sulfur, it was concluded that the pyrite had undergone thermal decomposition.

It is, therefore, interesting to consider that other techniques used to measure the rate of pyrite reduction by H_2 at high temperatures, such as chromatographic monitoring of H_2S production, would not yield accurate kinetic data unless precautions were taken to ensure that all sulfur was converted to H_2S. From Figure 13, it is seen that in 0.10 MPa H_2, thermal decomposition of pyrite is the predominate pathway at temperatures above approximately 775 K.

As the temperature is reduced to within the intermediate region shown on Figure 13, a different reaction appears to

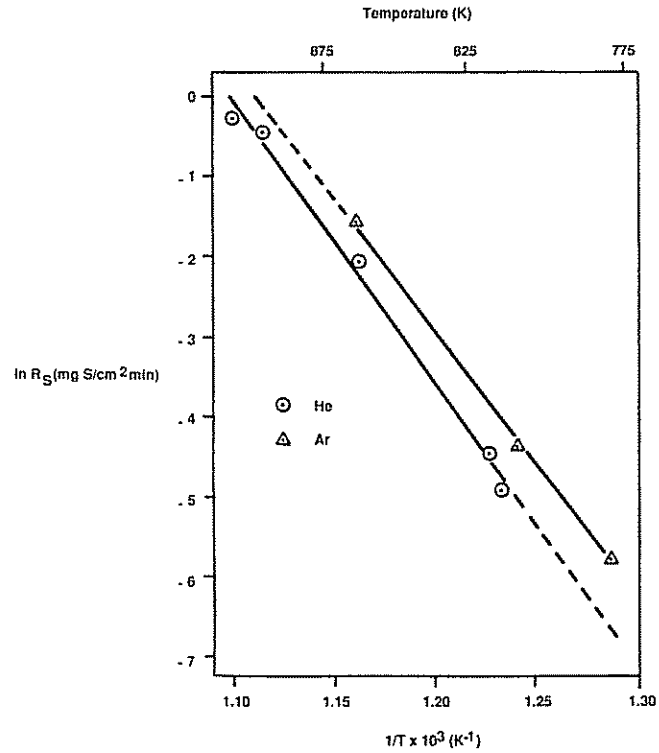

Fig. 12—Arrhenius plot of 210 × 250-μm Sonora pyrite decomposition in inert atmospheres at 0.8 MPa.

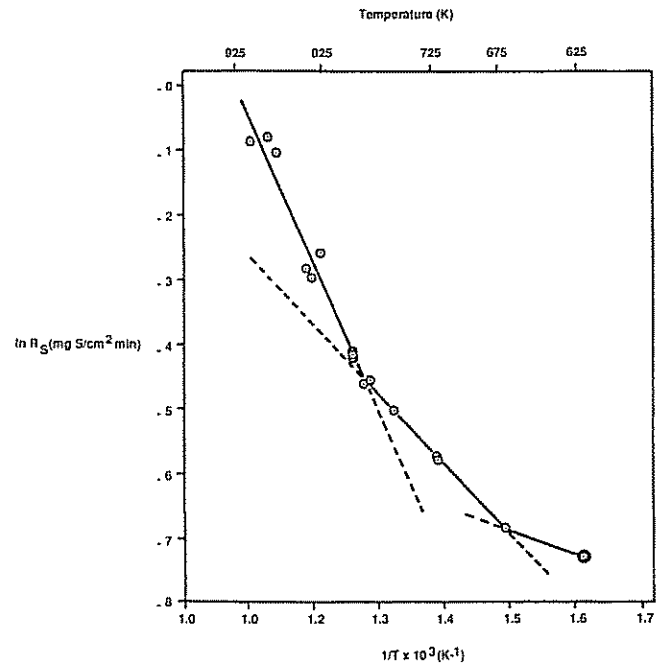

Fig. 13—Arrhenius plot of 210 × 250-μm Sonora pyrite decomposition in H_2 at 0.1 MPa (1 atm).

dominate the kinetics. In this region, an apparent activation energy of 88.7 kJ/mol was calculated. This corresponds well with the activation energy reported in the literature[21] for the diffusion of iron through pyrrhotite. This appears to be a likely rate-controlling step, as it was previously shown that a pyrrhotite layer forms on the exterior of the shrinking

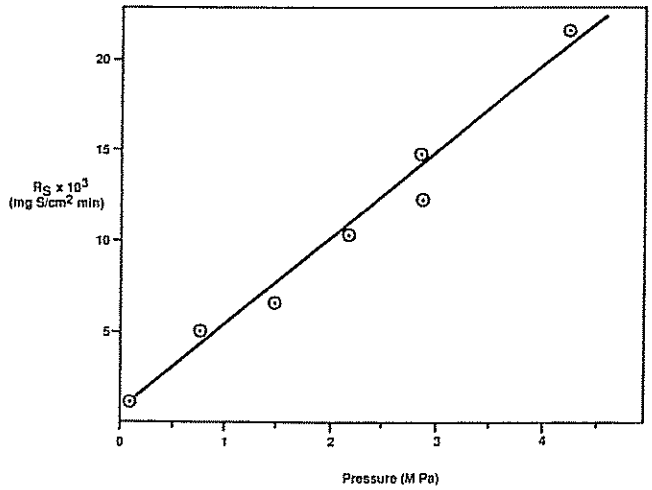

Fig. 14—Rate of reduction of 210 × 250-μm Sonora pyrite as a function of H_2 pressure at 673 K.

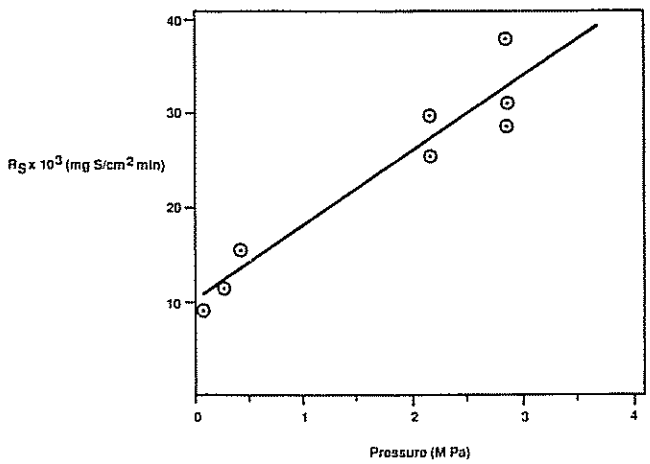

Fig. 15—Rate of reduction of 210 × 250-μm Sonora pyrite as a function of H_2 pressure at 778 K.

pyrite core. Recall that this pyrrhotite was found to be in equilibrium with pyrite and was always observable by X-ray diffraction, indicating that it always had a finite thickness.

The rate of diffusion of iron in pyrrhotites greatly exceeds the rate of sulfur diffusion.[21] As sulfur atoms leave the pyrite surface, it is envisioned that they are adsorbed onto the interior surface of the pyrrhotite layer. The iron in this pyrrhotite then diffuses inwardly, toward the sulfur, to accommodate the new atoms moving into the pyrrhotite structure. This process depletes iron atoms from the outer layer of the particle and liberates sulfur atoms into the flowing gas stream. The net effect, if one assumes the reference frame of the iron lattice, is that the sulfur appears to "diffuse" through the pyrrhotite layer. For ease of explanation, this process of iron diffusion and sulfur liberation will, at times, be referred to as "sulfur diffusion."

An apparent activation energy of 31.0 kJ/mol was found in the low-temperature region, below 670 K. The double circle surrounding the data point at 620 K in Figure 13 represents a duplicate experimental measurement. The reaction rate at this temperature was exceedingly slow, and

Table III. Kinetic Parameters for the Reduction of 210 × 250-μm Sonora Pyrite in 0.10 MPa H_2

Temperature Range (K)	$R_{s,0}$ (mg/cm² min)	E_{act} (kJ/mol)	Standard Deviation (kJ/mol)
910 to 780	1.1×10^{11}	195	12
780 to 670	8.5×10^{3}	89	2
670 to 620	2.7×10^{-1}	31	—

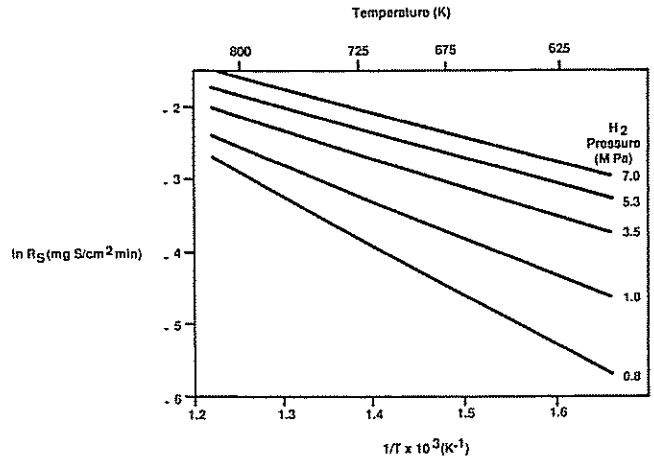

Fig. 16—Arrhenius plots of H_2 reduction of 210 × 250-μm Sonora pyrite at elevated pressure.

attempts to measure the rate at lower temperatures were infeasible due to the diminishing signal-to-noise ratio experienced on the strip chart recorder. The activation energy measured in this region corresponds well with the enthalpy reported for the expulsion of a sulfur atom from a pyrite lattice.[22] Evidence for this being a proper kinetic assignment comes from two points. It has been shown that pyrite can exist over a range of compositions from $FeS_{1.94}$ to $FeS_{2.01}$.[23] The second point to be noted is that, at low temperatures, very small extents of conversions are used in the analysis by the initial slope method.

In 4 hours reaction time, less than 10 pct of the initial weight was lost. At these temperatures, the linear region only extended to approximately 30 minutes, representing a conversion of approximately 1.3 pct. Since the conversion of pyrite to $FeS_{1.94}$ would only represent a conversion of 1.6 pct, it seems likely that this assignment is realistic.

The H_2 reduction of pyrite was investigated next at higher pressures. The specific reaction rates at 673 and 778 K, as a function of H_2 pressure, are shown in Figures 14 and 15, respectively. As can be seen in these figures, the reduction rate is directly proportional to the applied pressure. From a least-squares line through the data points, rates were calculated to produce the Arrhenius plot shown in Figure 16. It is seen that the apparent activation energy decreased with increasing pressure, reaching a value of 28 kJ/mol at 7.0 MPa. This value is in reasonable agreement with the value of 31 kJ/mol, calculated from the much more extensive measurements of the pyrite reduction rate at 7.0 MPa pressure performed by Garg,[24] and also agrees with the value reported for the expulsion of sulfur atoms from the pyrite lattice.[22]

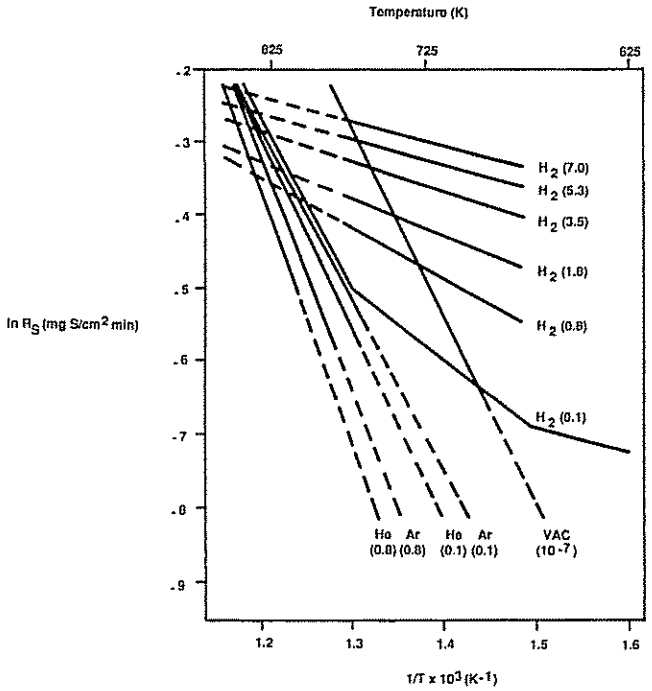

Fig. 17—Arrhenius plot of 210 × 250-μm Sonora pyrite reduction in various atmospheres at various pressures.

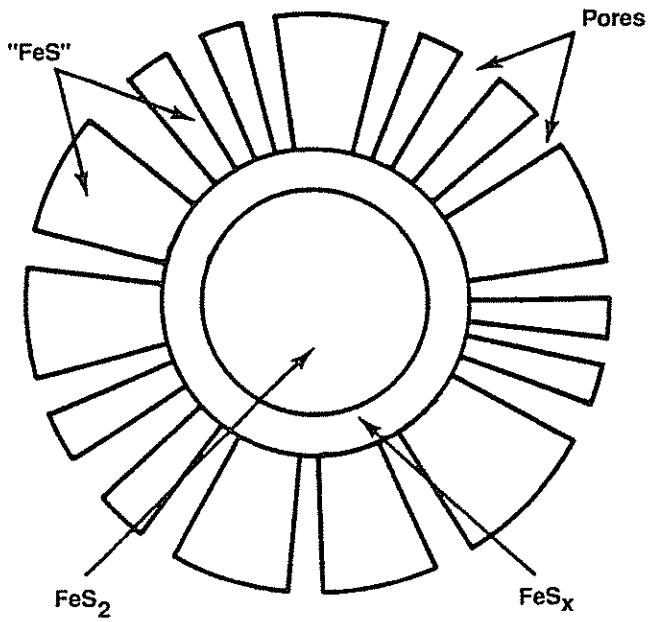

Fig. 18—Diagrammatic representation of a partially reduced pyrite particle showing topotactic transformation.

B. *Mechanistic Analysis*

From the data discussed previously, a mechanistic picture of the pyrite-to-pyrrhotite transformation can be proposed. A compilation of the Arrhenius plots reported in this article is shown in Figure 17, with the data points omitted for clarity. A schematic representation of a partially reduced pyrite particle is shown in Figure 18.

The first step in the transformation is the release of sulfur atoms from the pyrite lattice. An apparent activation energy of approximately 30 kJ/mol is assigned to this step. At this point, the sulfur atom is adsorbed on the surface where, if in an inert atmosphere, it can combine with another adsorbed sulfur atom and desorb as S_2; or, if in the presence of H_2, it can be abstracted as H_2S. This loss of sulfur causes the observed weight loss.

Eventually, sufficient sulfur is lost from the pyrite lattice that an outer layer converts to a pyrrhotite structure. Subsequent sulfur atoms released from the pyrite surface become first adsorbed onto the pyrite/pyrrhotite interface and then must diffuse through the FeS_x layer. (Recall that this is actually accomplished by the iron atoms undergoing inward diffusion.) The measured activation energy of approximately 90 kJ/mol is assigned to this step. The pyrrhotite through which the sulfur must first diffuse, FeS_x, is in equilibrium with the pyrite. Its composition is dependent only on the temperature, as the effective sulfur pressure in its local environment is sufficient to maintain the composition at the highest sulfur content thermodynamically allowable. Further away from the FeS_2/FeS_x interface and nearer to the particle surface, the composition may become lower in sulfur concentration due to desorption of S_2 or reaction with H_2.

The sulfur atoms, having diffused through the FeS_x layer, are now adsorbed on the FeS_x surface at the FeS_x/FeS interface. The expression FeS refers to any of the pyrrhotites in the solid-solution region; that is, those whose composition is intermediate between that of the pyrrhotite in equilibrium with pyrite and troilite, stoichiometric FeS.

The FeS_x/FeS interface is moving inwardly, following the FeS_2/FeS_x interface. The rates of migration of the two interfaces are not identical. As the interfaces progress inwardly, a topotactic transformation takes place and a macroporous structure is formed. This porous layer on the exterior of the particle brings about the tenfold increase in specific surface area reported[16] when pyrite is reduced to pyrrhotite. The porosity is a result of the 25 pct reduction in molar volume of the solid as pyrite (24 cc/mol) is converted to pyrrhotite (18 cc/mol).

The "migrating sulfur atoms" eventually diffuse to the surface of the FeS layer and combine, if in an inert atmosphere, to form S_2 molecules. These molecules then desorb from the surface, diffusing away from the particle through the pores. The measured activation energy of 200 kJ/mol is assigned to this desorption step. This step is also assigned to be the rate-controlling step for the decomposition *in vacuo* and in inert atmospheres. It is also the rate-controlling step at high temperatures in the presence of H_2.

Provided that the flux of desorbing S_2 is not so great as to inhibit the inward diffusion of H_2, the hydrogen can facilitate the removal of sulfur atoms from the FeS surface. This process is so much more efficient at removing sulfur than S_2 formation and desorption that the rate-determining step changes to become diffusion of sulfur through the pyrrhotite layer. This accounts for the reduction in apparent activation energy from approximately 200 to approximately 90 kJ/mol.

As the pressure of H_2 is increased, so is the rate of sulfur removal from the surface. This increases the concentration gradient controlling the solid-state diffusion. At a pressure of 7.0 MPa, the rate at which sulfur diffuses through the pyrrhotite layer is increased to the extent that it is no longer

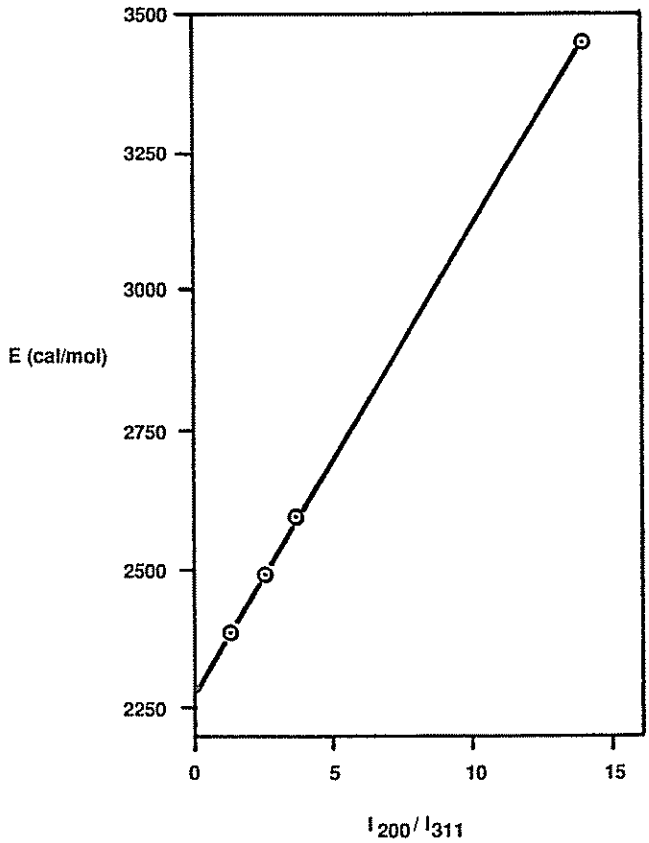

Fig. 19—Heats of adsorption of Kr on pyrites as a function of increasing amounts of {100} crystallographic faces.[20]

Table IV. Specific Reaction Rates, R_s, for the Reduction of Four Pyrite Samples in 1.5 MPa H_2 at 693 K

Sample	Designation*	Particle Size (μm)	Specific Surface Area (cm^2/mg)	R_s (mg/cm^2 min)
Sonora	a	210 × 250	0.17	0.027
Sonora	b	44 × 53	0.27	0.089
Rico	c	<74	0.98	0.043
N.C.	d	210 × 250	0.095	0.076

*Refers to data points shown in Fig. 20.

the rate-determining step. The slow step in the series reaction sequence is now the formation of sulfur atoms by their expulsion from the pyrite lattice. This step has an apparent activation energy of approximately 30 kJ/mol.

Thus, there are three different steps which exert control over the rate of the pyrite-to-pyrrhotite transformation. The rate which is experimentally measured is dependent upon temperature, pressure, and atmosphere. With such a diversity of possible rate-controlling processes, it is not surprising that such a wide variation in activation energies for the reduction of pyrite to pyrrhotite has been reported in the literature. This study also emphasizes the desirability of performing kinetic analyses over as wide a temperature range as possible.

Two additional points of interest can be noted from the kinetic analyses presented in Figure 17. The first point to note is that in the presence of H_2, the same apparent activation energy (30 kJ/mol) was found at very low temperatures, where no significant pyrrhotite layer was yet present, and under conditions of very high pressure in the presence of a pyrrhotite layer. In both cases, the rate-determining step was attributed to the expulsion of sulfur from the pyrite lattice. The rates of reaction of 673 K are different by approximately 3.5 orders of magnitude. Since the same activation energy was found, the difference in rate must be attributed to entropy changes, as opposed to enthalpy changes, and are, therefore, manifested in the pre-exponential term of the rate expression. Numerically, this entropy difference was calculated to be approximately 10.5 J/mol K. This increase in entropy may be due to the effect of hydrogen being solubilized in the solid, or it may be the result of some lattice strain imposed on the crystal.

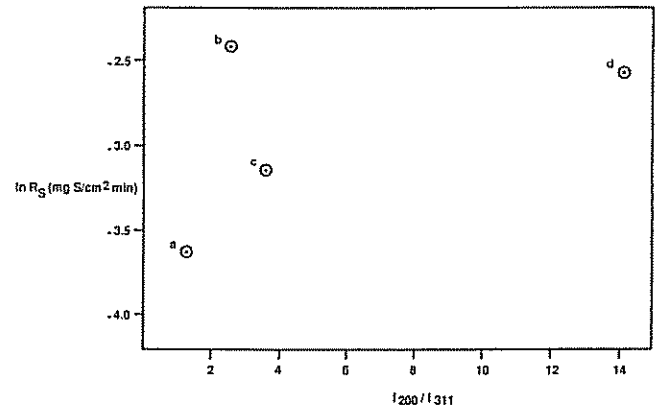

Fig. 20—Rate of reduction of various pyrites in 1.5 MPa H_2 at 693 K as a function of X-ray intensity ratio.

The second point to note is that in the analysis of reactions occurring in series, a shift in the measured activation energy from a higher to a lower value is generally achieved by an increase in temperature.[20] In this study, it became apparent that this behavior can also be accomplished by increasing the pressure. In the case of pyrite reduction in 0.1 MPa H_2, the rate-determining step is a solid-state diffusion with a measured activation energy of 90 kJ/mol. When this pressure is increased to 7.0 MPa H_2 at the same temperature (720 K, for example), the rate-determining step shifts to a previous step of the series—the sulfur atom expulsion from the pyrite lattice—with a measured activation energy of 30 kJ/mol.

C. *Comparison of Reactivity of Different Pyrites*

It was previously shown[20] that the heat of adsorption of Kr on pyrite at 77 K could be correlated with the relative amounts of {100} crystallographic faces present, as indicated by an $I_{(200)}/I_{(311)}$ intensity ratio obtained from X-ray diffraction analysis. This correlation is reproduced in Figure 19. A similar-type correlation was sought between the pyrite reactivity to H_2 and the extent of {100} crystallographic faces present.

To test this assumption, the rates of reduction of the same pyrite samples shown in Figure 19 were measured at 693 K in 1.5 MPa H_2. These conditions were chosen to ensure that the measured rate was due only to H_2 reduction (*cf.* Figure 17). The values of the specific reaction rates, along with the particle sizes and specific surface areas measured by Kr adsorption, are given in Table IV. The specific re-

Table V. Chemical Analysis of Four Pyrite Samples

Element	Concentration (ppm)			
	Sonora 210 × 250 μm	Sonora 44 × 53 μm	Rico <74 μm	N.C. 210 × 250 μm
Al	*	*	3000	*
Ba	*	*	<10	*
Ca	*	*	2000	*
Co	<100	<100	300	150
Cu	<100	<100	200	18
Mg	*	*	70	*
Mn	*	*	30	10
Ni	*	*	30	170
Si	*	*	1 to 4 pct	*
Sr	*	*	20	*
Ti	*	*	30	*
V	*	*	<10	*
Y	*	*	<30	*
Zn	*	*	*	24
Zr	*	*	<20	*

*Indicates concentrations below limits of detection.

action rates (R_s) are plotted as a function of the $I_{(200)}/I_{(311)}$ intensity ratio in Figure 20. As can be seen, the correlation was not linear. It should be noted, however, that when the same pyrite sample was ground to a smaller particle size (samples a and b), the relative amount of {100} crystallographic faces increased, as did the specific reaction rate for H_2 reduction. Samples c and d have greater amounts of {100} faces exposed, but their reactivity to H_2 reduction is significantly reduced below an extrapolation of points a and b.

Examination of the impurity concentrations listed in Table V suggests that the increasing concentration of impurities in samples c and d may be responsible for the reduction in rates. The impurity-sulfur bond is stronger for most of the impurities than the iron-sulfur bond. As these experiments were conducted in the region where solid-state diffusion of sulfur was the rate-controlling step, it might be expected that the rate of diffusion of sulfur through impurity-containing solid would be lessened. This would then lead to the observed reduction in the rate at which hydrogen would remove sulfur from the surface.

IV. SUMMARY

The kinetics of the reduction of pyrite to form pyrrhotite were investigated by TGA over a range of temperatures (620 to 973 K) and pressures (0.2 Pa to 7.0 MPa) in atmospheres of H_2, He, Ar, and *in vacuo*. Results of this study led to a mechanistic description of the process. This description can be summarized with the use of chemical equations in the following manner.

In inert atmospheres of He and Ar, as well as *in vacuo*, pyrite is thermally reduced to a pyrrhotite of specific composition *via* the following equation:

$$FeS_2 \longrightarrow FeS_x + (2 - x)\ S \qquad [20]$$

In the local environment of the pyrite/pyrrhotite interface, the sulfur fugacity is of such magnitude that the FeS_x formed is always the pyrrhotite which is in equilibrium with pyrite. Thus, the value of x in FeS_x is only a function of temperature and can be calculated from Eq. [8] or [9]. The rate-determining step for this reaction was found to be the desorption of sulfur from the surface. An apparent activation energy of approximately 200 kJ/mol was observed.

As the sulfur fugacity is reduced below that required for FeS_x equilibrium, the pyrrhotite begins to lose additional sulfur as its composition traverses the region of solid solution. This can be described as

$$FeS_x \longrightarrow FeS_y + (1 - y)\ S \qquad [21]$$

where $1.0 < y < x$.

The liberated sulfur is more accurately expressed as $1/n\ S_n$, rather than simply S. Sulfur can exist in various polymeric forms where n is an integer between 2 and 8. The relative proportions of the various forms present depends upon both the partial pressure of sulfur and the temperature. It can be seen in Figure 1 that the highest equilibrium sulfur pressure to be experienced in this investigation is of the order of 2×10^{-4} MPa. It has been shown[11] that under these conditions, greater than 95 pct of the sulfur which is liberated in the temperature and pressure ranges investigated in this study exists in the form of S_2.

In the presence of H_2, different reactions can take place. The sulfur which is liberated *via* Reactions [20] and [21] can combine with hydrogen to form hydrogen sulfide.

$$(2 - x)\ S + (2 - x)\ H_2 \longrightarrow (2 - x)\ H_2S \qquad [22]$$

$$(x - y)\ S + (x - y)\ H_2 \longrightarrow (x - y)\ H_2S \qquad [23]$$

Under the appropriate conditions, the hydrogen can abstract sulfur directly from the surface of the solids. For example, at very low extents of conversion and prior to the formation of an external layer of pyrrhotite, hydrogen can abstract sulfur from the pyrite surface:

$$FeS_2 + zH_2 \longrightarrow FeS_{(2-z)} + zH_2S \qquad [24]$$

where the value of z is between 0.00 and 0.04. This reaction was found to proceed with an apparent activation energy of approximately 30 kJ/mol, attributable to the enthalpy involved in the expulsion of a sulfur atom from the pyrite lattice.

Once a pyrrhotite layer has formed surrounding the pyrite core, sulfur is removed from the surface according to the following equations:

$$FeS_2 + (2 - x)\ H_2 \longrightarrow FeS_x + (2 - x)\ H_2S \qquad [25]$$

$$FeS_x + (x - y)\ H_2 \longrightarrow FeS_y + (x - y)\ H_2S \qquad [26]$$

$$FeS + H_2 \longrightarrow Fe + H_2S \qquad [27]$$

Reaction [27] has been reported to occur at temperatures in excess of 1175 K.[9] Reaction [26] is the most commonly observed reduction step. It has an apparent activation energy of approximately 90 kJ/mol and has as a rate-determining step the diffusion of iron through the pyrrhotite layer, which, in effect, frees sulfur atoms from the opposite face. Once the sulfur atoms "reach the surface," they are readily removed by the H_2. The rate of this removal by H_2 is more rapid than the previously described process of S_2 desorption from the surface.

Reaction [25], the H_2 reduction of pyrite in the presence of a pyrrhotite layer, is much more complicated than is

implied by the simple equation. At a H_2 pressure of 0.10 MPa and at temperatures below 775 K, the gas is not in direct contact with the pyrite surface. Sulfur is liberated from the pyrite *via* Reaction [20]. It then diffuses through the FeS_x layer, maintaining the FeS_2/FeS_x equilibrium, and is removed by H_2 at the exterior surface, as in Eq. [26]. The solid-state diffusion is the slow step in this series, and is, thus, the rate-determining step. The apparent activation energy for this diffusion is approximately 90 kJ/mol.

Recall that the diffusing species is actually iron, moving inwardly. The "apparent diffusion" of sulfur is the result of viewing the migration from a reference frame fixed on the iron atoms.

As the pressure of H_2 is increased above ambient conditions, the rate of sulfur removal is found to increase proportionately. This increased rate of sulfur removal causes an increase in the sulfur concentration gradient in the pyrrhotite. The increased gradient allows for more rapid diffusion. At approximately 7.0 MPa, the rate of sulfur diffusion is no longer the slow step, and rate control shifts to the expulsion of sulfur from the pyrite lattice. This step has an apparent activation energy of approximately 30 kJ/mol. It is under these conditions that the H_2 reduction of pyrite follows Reaction [25].

As the temperature is increased, reaction control will shift back to a thermal process unless higher H_2 pressure is applied. For example, at temperatures above 775 K in 0.10 MPa H_2, the sulfur vapor is thermally desorbing from the surface at such a rate that the inward diffusion of H_2 is restricted. It is found that the rate at which pyrite is thermally transformed into pyrrhotite is suppressed by the physical existence of an increased pressure. Simultaneously, however, an increasing H_2 pressure increases the chemical reduction rate by abstracting sulfur atoms from the surface.

ACKNOWLEDGMENTS

Partial support of this study for JML, Jr. from the United States Department of Education in the form of a Mining, Minerals, and Mineral Fuel Conservation Fellowship and the United States Department of the Interior in the form of a Mining and Mineral Resources Research Institute Fellowship is appreciated. Helpful discussions were held with Professor H.L. Barnes.

REFERENCES

1. G.M. Schwab and J. Philinis: *J. Am. Chem. Soc.*, 1947, vol. 69 (11), pp. 2588-96.
2. A.W. Coats and N.F.H. Bright: *Can. J. Chem.*, 1966, vol. 44, pp. 1191-95.
3. B.K. Guha and G. Narsimhan: *Chem. Eng.*, 1972, vol. 3, pp. 145-55.
4. P.A. Montano: *Fuel*, 1981, vol. 60, pp. 703-11 and 712-16.
5. M.L. Vestal and W.H. Johnson: *ACS Div. Fuel Chem., Preprints*, 1970, vol. 14 (1), pp. 1-11.
6. P.R. Solomon: Research Report No. R76-952588-2, United Technologies Research Center, East Hartford, CT, Apr. 1977, pp. 12-19.
7. A. Attar: *Coal Processing Technol.*, 1978, vol. 4, pp. 26-34.
8. T.D. Padrick, M.G. Thomas, and F.V. Stohl: Research Report No. SAND80-1426, Sandia National Laboratories, Albuquerque, NM, June 1980.
9. I.G. Gallo: *Ann. Chim. Applicata*, 1927, vol. 17, p. 39; also appeared in *Chem. Abstr.*, 1927, vol. 21, p. 1243.
10. K. Niwa, Y. Katsufuji, and T. Maekawa: *Nippon Kinsoku Gakkai Shi*, 1953, vol. 17, p. 431.
11. S.D. Scott: *Sulfide Mineralogy, Short Course Notes*, Mineralogical Society of America, Washington, D.C., 1974, vol. 1, ch. 4.
12. P. Toulmin and P.B. Barton: *Geochim. Cosmochim. Acta*, 1964, vol. 28, pp. 641-71.
13. S.D. Scott and H.L. Barnes: *Econ. Geol.*, 1971, vol. 66, pp. 653-69.
14. J.M. Lambert, Jr., G. Simkovich, and P.L. Walker, Jr.: *Fuel*, 1980, vol. 59, pp. 687-90.
15. G.G. Zahuranec: Master's Thesis, The Pennsylvania State University, University Park, PA, 1977.
16. J.M. Lambert, Jr., P.L. Walker, Jr., A.J. Perotta, J.P. McCullough, and H. Beuther: *Fuel*, 1983, vol. 72, pp. 1474-80.
17. G.M. Rosenblatt: in *Treatise on Solid State Chemistry*, N.B. Hannay, ed., Plenum Press, New York, NY, 1976, vol. 6A, ch. 3.
18. C.N. Satterfield and T.K. Sherwood: *The Role of Diffusion in Catalysis*, Addison-Wesley, Reading, MA, 1963.
19. E.T. Turkdogan, P. Grieveson, and L.S. Darken: *J. Phys. Chem.*, 1963, vol. 67, pp. 1647-54.
20. J.M. Lambert, Jr.: Ph.D. Thesis, The Pennsylvania State University, University Park, PA, 1982.
21. R.H. Condit, R.R. Hobbins, and C.E. Birchenall: *Oxid. Met.*, 1974, vol. 8 (6), pp. 409-53.
22. R.S.B. Chrystall: *Trans. Faraday Soc.*, 1965, vol. 61 (8), pp. 1811-15.
23. F.G. Smith: *Am. Mineral.*, 1942, vol. 27 (1), pp. 1-19.
24. D. Garg: Air Products and Chemicals, Allentown, PA, private communication, 1979.